Proceedings of the ASME 2012 Pressure Vessels & Piping Division Conference
PVP2012
July 15-19, 2012, Toronto, Ontario, CANADA

PVP2012-78119

ADDITIONAL STRESS AND FRACTURE MECHANICS ANALYSES OF PRESSURIZED WATER REACTOR PRESSURE VESSEL NOZZLES

Matthew Walter
Structural Integrity Associates, Inc.
Centennial, CO, USA
mwalter@structint.com

Shengjun Yin
Oak Ridge National Laboratory
Oak Ridge, Tennessee, USA
yins@ornl.gov

Gary L. Stevens
U.S. Nuclear Regulatory Commission
Washington, DC, USA
gary.stevens@nrc.gov

Daniel Sommerville
Structural Integrity Associates, Inc.
Seattle, WA, USA
dsommerville@structint.com

Nathan Palm
Westinghouse Electric Company
Cranberry Township, Pennsylvania, USA
palmn@westinghouse.com

Carol Heinecke
Westinghouse Electric Company
Cranberry Township, Pennsylvania, USA
heineccc@westinghouse.com

ABSTRACT

In past years, the authors have undertaken various studies of nozzles in both boiling water reactors (BWRs) and pressurized water reactors (PWRs) located in the reactor pressure vessel (RPV) adjacent to the core beltline region. Those studies described stress and fracture mechanics analyses performed to assess various RPV nozzle geometries, which were selected based on their proximity to the core beltline region, i.e., those nozzle configurations that are located close enough to the core region such that they may receive sufficient fluence prior to end-of-life (EOL) to require evaluation of embrittlement as part of the RPV analyses associated with pressure-temperature (P-T) limits. In this paper, additional stress and fracture analyses are summarized that were performed for additional PWR nozzles with the following objectives:

- To expand the population of PWR nozzle configurations evaluated, which was limited in the previous work to just two nozzles (one inlet and one outlet nozzle).
- To model and understand differences in stress results obtained for an internal pressure load case using a two-dimensional (2-D) axi-symmetric finite element model (FEM) vs. a three-dimensional (3-D) FEM for these PWR nozzles. In particular, the ovalization (stress concentration) effect of two intersecting cylinders, which is typical of RPV nozzle configurations, was investigated.
- To investigate the applicability of previously recommended linear elastic fracture mechanics (LEFM) hand solutions for calculating the Mode I stress intensity factor for a postulated nozzle corner crack for pressure loading for these PWR nozzles.

These analyses were performed to further expand earlier work completed to support potential revision and refinement of Title 10 to the U.S. Code of Federal Regulations (CFR), Part 50, Appendix G, “Fracture Toughness Requirements,” and are intended to supplement similar evaluation of nozzles presented at the 2008, 2009, and 2011 Pressure Vessels and Piping (PVP) Conferences. This work is also relevant to the ongoing efforts of the American Society of Mechanical Engineers (ASME) Boiler and Pressure Vessel (B&PV) Code, Section XI, Working Group on Operating Plant Criteria (WGOPC) efforts to incorporate nozzle fracture mechanics solutions into a revision to ASME B&PV Code, Section XI, Nonmandatory Appendix G.

NOMENCLATURE

2-D	=	Two Dimensional
3-D	=	Three Dimensional
ASME	=	American Society of Mechanical Engineers
BIE/IF	=	Boundary Integral Equation / Influence Function
B&PV	=	Boiler and Pressure Vessel
B&W	=	Babcock and Wilcox
BWR	=	Boiling Water Reactor
CE	=	Combustion Engineering
CF	=	Correction Factor
CFR	=	Code of Federal Regulations
EOL	=	End of Life
FEA	=	Finite Element Analysis
FEM	=	Finite Element Model
IR	=	Inside Radius
LEFM	=	Linear Elastic Fracture Mechanics
PWR	=	Pressurized Water Reactor
RPV	=	Reactor Pressure Vessel
SCF	=	Stress Concentration Factor
SI	=	Safety Injection
W	=	Westinghouse
WGOPC	=	Working Group on Operating Plant Criteria
D_i	=	Inside Diameter, in
D_o	=	Outside Diameter, in
K_I	=	Applied Stress Intensity Factor, ksi-in^2
K_t	=	Stress Concentration Factor
P	=	Internal Pressure, psig or ksi
R	=	RPV Inside Radius, in
r	=	Nozzle Bore Radius, in
t	=	RPV Shell Thickness, in
β	=	Shell Parameter
ν	=	Poison's Ratio

INTRODUCTION

The finite element method is commonly used for stress analysis of pressure vessel components, often for input into fracture mechanics or fatigue analyses. 2-D axi-symmetric models are often used, when appropriate, to save time and cost associated with performing these stress analyses. Since a 2-D axi-symmetric FEM requires fewer nodes to adequately model the geometry compared to a 3-D FEM, the construction, solution and postprocessing times are less than those required for a 3-D FEM. The benefits of using a 2-D FEM become significant when performing transient or non-linear analyses. Further, many of the operating nuclear plants have design basis nozzle stress analyses which were performed using 2-D axi-symmetric models due to computational limits present during the timeframe when those older analyses were performed. Therefore, information from such evaluations is available and can be used without requiring development of newer, more detailed models.

Modeling a RPV nozzle with a 2-D FEM has the effect of representing the vessel as a spherical shell rather than a cylindrical shell. This simplification affects the stress distribution in the nozzle blend radius region; therefore, specific action must be taken to correct the 2-D axi-symmetric analysis results for certain types of loading, including pressure loading. Away from the nozzle corner and into the nozzle bore, the 2-D axi-symmetric modeling assumption is representative of the actual configuration so the stresses are approximated correctly by the model. In the RPV shell, remote from the nozzle corner, hand calculations are sufficient to calculate the stresses from applied mechanical loads; thus, the modeling simplification does not present significant problems for the RPV wall region.

Significant work has been performed in the past to characterize nozzle stress distributions for internal pressure and external loads [1, 2], provide nozzle stress concentration factors for various loads [2, 3], and to correct 2-D axi-symmetric nozzle results to better represent the 3-D configuration of the geometry [3, 4, 5, 6, 7, 8]. Additional work can be found dating back to the 1960's and 1970's on this topic. The references identified here do not form a comprehensive list of the literature on this topic; rather, they are simply provided as a sample of the available literature. The present paper expands on this work documented in previous PVP papers presented in 2008, 2009, and 2011, and focuses further attention on PWR nozzle configurations.

PREVIOUS CORRECTION TECHNIQUES

Sommerville and Walter [5] present a method for correcting 2-D stress distributions at the nozzle corner using hand book stress concentration factors (SCFs). The method was shown to be conservative by comparing corrected path stress distributions obtained using the proposed methodology to those extracted from a 3-D FEM for nine (9) BWR nozzle models. The methodology is summarized as follows:

1. Build the 2-D axisymmetric nozzle FEM using the correct dimensions without any geometric correction factors applied to the inside radius of the vessel.
2. Calculate the expected 3-D SCF at the nozzle blend radius using the SCF equations given in Pilkey & Pilkey [9], which are taken from Van Dyke [10], as follows:

For $0 \le \beta \le 2$, (1)

$$K_t(\beta) = 2.5899 + 0.8002 \cdot \beta + 4.0112 \cdot \beta^2 - 1.8235 \cdot \beta^3 + 0.3751 \cdot \beta^4$$

For $2 \le \beta \le 4$,

$$K_t(\beta) = 8.3065 - 7.1716 \cdot \beta + 6.70 \cdot \beta^2 - 1.35 \cdot \beta^3 + 0.1056 \cdot \beta^4$$

$$\beta = \frac{\left[3 \cdot \left(1 - \nu^2\right)\right]^{0.25}}{2} \cdot \left(\frac{r}{\sqrt{R \cdot t}}\right)$$

3. Correct the path stresses obtained from the 2-D axi-symmetric FEM by uniformly scaling the path stresses by the nozzle SCF obtained using the equations in Step 2.
4. Alternatively, a slightly more accurate and less conservative correction factor (CF) can be obtained by determining the SCF inherent in the 2-D axi-symmetric FEM and calculating the CF as follows:

$$CF = 2 \cdot \frac{SCF_{3D}}{SCF_{2D}} \qquad (2)$$

This methodology was shown to provide a reasonable and conservative stress correction factor for membrane plus bending stresses, as well as total stresses at the nozzle corner [5].

Yin, et al. [8] recommend a bounding factor of 3.1 for nozzles with rounded inside corners and 3.5 for nozzles with special discontinuities or sharp inside corners, such as the PWR outlet nozzle and the BWR instrument nozzle. They also acknowledge that this value agrees with the ASME B&PV Code, Section III [11] Stress Index for nozzles. It is also notable that these values are both near the value of 3.2 recommended by Truitt and Raju [6] for LWR nozzles.

PWR NOZZLE GEOMETRIES INVESTIGATED

For this paper, four additional nozzle geometries were selected for analysis, which represent typical geometries for PWR nozzles located adjacent to the RPV core region:

- Combustion Engineering (CE) RPV outlet nozzle
- Westinghouse (W) RPV safety injection (SI) nozzle
- Babcock and Wilcox (B&W) RPV core flood nozzle
- B&W RPV inlet nozzle

Figures 1 through 4 show the as-modeled dimensions for each of these nozzle geometries. Table 1 summarizes the critical dimensions for each nozzle.

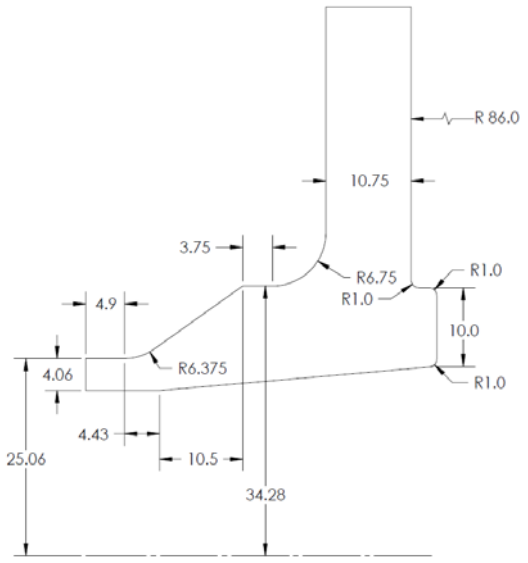

FIGURE 1: CE RPV OUTLET NOZZLE GEOMETRY

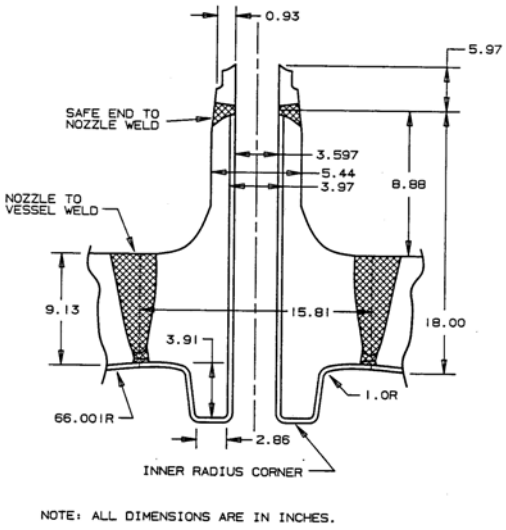

FIGURE 2: WESTINGHOUSE RPV SI NOZZLE GEOMETRY

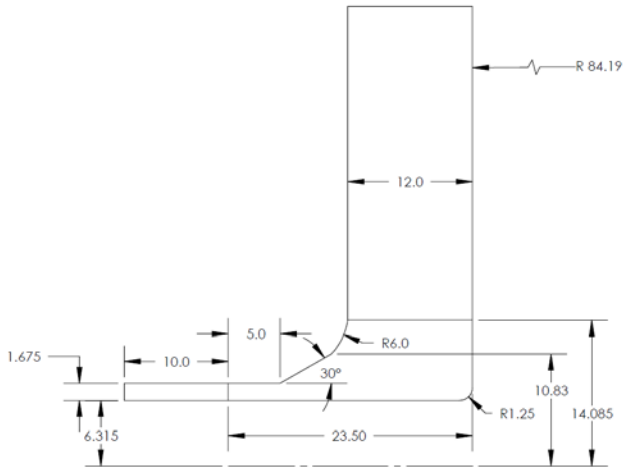

FIGURE 3: B&W RPV CORE FLOOD NOZZLE GEOMETRY

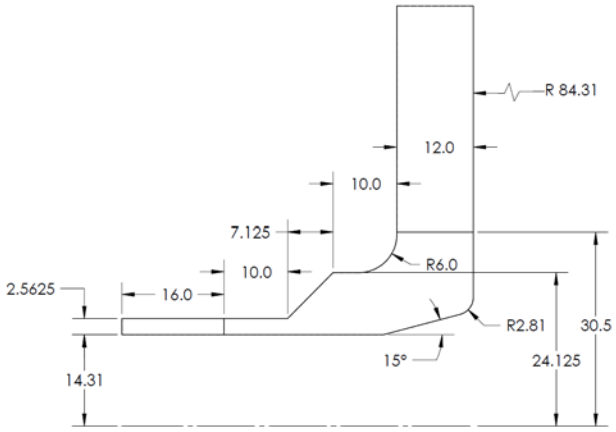

FIGURE 4: B&W RPV INLET NOZZLE GEOMETRY

TABLE 1: NOZZLE DIMENSIONS CONSIDERED IN STUDY

Nozzle	(ALL UNITS IN INCHES) RI_{vess}	t_{vess}	RI_{pipe}	BR_{inner}
CE RPV OUTLET	86.00	10.75	21.00	1.00
W RPV SI	66.00	9.13	1.80	0.50
B&W RPV CORE FLOOD	84.19	12	6.315	1.25
B&W RPV INLET	84.31	12	14.31	2.81

FINITE ELEMENT MODELS

Eight FEMs (four 2-D and four 3-D) were constructed for the selected nozzle geometries. The CE and W nozzles were modeled using ABAQUS [12], and the B&W nozzles were modeled using ANSYS [13]. The 2-D analyses were performed using 8-node axi-symmetric quadratic elements (CAX8 in ABAQUS and PLANE82 in ANSYS). The 3-D analyses were performed using 20-node solid quadratic elements (C3D20 in ABAQUS and SOLID95 in ANSYS). Figures 5 through 8 show the 3-D finite element mesh for each of the modeled nozzles. Figure 9 shows a typical 2-D mesh.

The extent of the RPV shell included in each model was defined such that boundary effects did not introduce non-representative effects in the finite element analysis (FEA) solution at the nozzle inside corner region. A 1,000 psig internal pressure "unit" load case was considered for this work so that results could easily be scaled to other pressures. For each model, the pressure load was applied on the inside surface of the RPV wall and nozzle bore. A blow-off or "cap" membrane load was applied to the piping end of the model to simulate the closed-end effects of the attached piping. Symmetry boundary conditions ("roller" conditions) were applied to the end of the RPV wall in the 2-D models. Symmetry boundary conditions were also applied on both of the vertical edges in the 3-D models. The lower horizontal edge in the 3-D models was fixed in the axial degree of freedom. A blow-off membrane load was applied to the piping edge in the 3-D models. Figures 10 and 11 show the boundary conditions and applied loads for a representative 2-D and 3-D model, respectively. The blow-off loads were calculated for the piping and RPV using the following formula:

$$P_{BlowOff} = \frac{P \cdot D_i^2}{D_o^2 - D_i^2} \quad (3)$$

A typical Poison's ratio value of 0.3 was used for all materials. The materials and Young's modulus values for each of the four nozzles are provided in Table 2.

TABLE 2: MATERIAL PROPERTIES

Nozzle	Component	Material	E x10^6 psi
CE RPV OUTLET	Vessel	SA-533 Grade B	29.2
	Vessel-to-Forging Weld	SA-508-64 Class 2	27.8
	Forging	SA-508-64 Class 2	27.8
	Safe End	SA-336-65 F8m	28.3
WESTINGHOUSE RPV SI	Vessel	SA-533 Grade B	29.2
	Vessel-to-Forging Weld	SA-508-64 Class 2	27.8
	Forging	SA-508-64 Class 2	27.8
	Safe End	SA-336-65 F8m	28.3
B&W RPV CORE FLOOD	Vessel	SA-508-64 Class 2	27.8
	Vessel-to-Forging Weld	SA-508-64 Class 2	27.8
	Forging	SA-508-64 Class 2	27.8
	Safe End	SA-336-65 F8m	28.3
B&W RPV INLET	Vessel	SA-508-64 Class 2	27.8
	Vessel-to-Forging Weld	SA-508-64 Class 2	27.8
	Forging	SA-508-64 Class 2	27.8
	Safe End	SA-106 Grade C	29.2

STRESS ANALYSIS

Figures 12 and 13 show contour plots of the 2-D and 3-D hoop stress due to the unit pressure load for a representative nozzle. Figures 14 and 15 show the unique case of the W SI nozzle which has the highest stress intensity in the nozzle bore. Note that a finite element mesh density check was performed for all models such that the mesh selected for analysis showed asymptotic convergence of total stress in the region of interest. Figures 16 through 19 show the paths defined for nozzle corner path stress extraction for each 3-D model. The stress paths begin at the node in the nozzle corner with the highest pressure hoop stress and extend through the nozzle corner region to the outside surface of the vessel wall at an angle of 45 degrees to the nozzle longitudinal axis. These paths were defined consistent with the common assumption of postulating a quarter-circular crack at the inside corner of a nozzle. This assumption was made to be consistent with the approximate location of largest pressure stress in most RPV nozzle designs; thus, it provides the path with largest crack driving force.

Therefore, the nozzle corner location is expected to result in the bounding LEFM evaluation for RPV integrity issues. The stress contour results from this investigation reveal that this assumption is appropriate for the CE RPV Outlet, B&W RPV Core Flood and B&W RPV Inlet nozzles; however, the nozzle corner does not coincide with the location of maximum stress for the W RPV SI nozzle. Due to the unique geometry characteristics of this nozzle, the stresses are compressive at the nozzle corner. As shown in Figures 14 and 15, the highest stressed region for this nozzle occurs along the nozzle bore for pressure loading.

Figures 16 through 19 plot the path stress distributions obtained from the 2-D and 3-D FEA of the CE RPV Outlet, W RPV SI, B&W RPV Core Flood, and B&W RPV Inlet nozzles, respectively. Also shown on these figures are the 2-D path stresses corrected using the CF calculated according to the method suggested by Sommerville and Walter [5]. Table 3 summarizes the CF determined from the FEA results directly as well as those calculated using Sommerville and Walter [5], for each nozzle design considered. These CF can be compared with the bounding correction factors suggested in Yin, et al. [8] and Truitt and Raju [6].

TABLE 3: NOZZLE CORRECTION FACTORS

	B&W RPV Core Flood	B&W RPV Inlet	W RPV SI	CE RPV Outlet
2D Hoop Stress, psi	7,547	6,723	7,264	7,600
3D Hoop Stress, psi	21,278	22,279	19,070	24,800
CF from FEA	2.82	3.31	2.63	3.26
$r_{i,pipe}$, in	6.315	14.31	1.799	21
$R_{i,vess}$, in	84.19	84.31	66	86
t_{vess}, in	12	12	9.13	10.75
v	0.3	0.3	0.3	0.3
β	0.13	0.29	0.05	0.44
CF [5]	2.75	3.12	2.64	3.59

NOZZLE FRACTURE MECHANICS EVALUATIONS

One of the objectives of the current investigation was to evaluate the applicability of the influence function LEFM solution being considered by the WGOPC for inclusion in ASME B&PV Section XI, Nonmandatory Appendix G to the PWR nozzle designs considered herein. The nozzle LEFM solution of interest is defined by the following Boundary Integral Equation / Influence Function (BIE/IF) solution:

$$K_I = \sqrt{\pi a}\left[0.706A_0 + 0.537\left(\frac{2a}{\pi}\right)A_1 + 0.448\left(\frac{a^2}{2}\right)A_2 + 0.393\left(\frac{4a^3}{3\pi}\right)A_3\right] \quad (4)$$

where:

K_I is the applied Mode I stress intensity factor for a quarter circular crack, ksi-in$^{0.5}$,

a is the ¼ wall thickness postulated flaw depth, in,

A_0, A_1, A_2 and A_3 are the polynomial curve fit coefficients for the nozzle corner path applied stress distribution.

The rationale for selecting the solution given by Eq. (4) is discussed in References [8, 14, 15]. The adequacy of this solution has been investigated numerous times, including discussion in References [8, 14, 15, 16]

For the purposes of this investigation, the ¼ wall thickness postulated flaw depth dimension selected for LEFM analysis is defined as ¼ of the 45-degree path length through the nozzle corner [15]. Table 4 summarizes the polynomial curve fit coefficients for all pressure stress distributions considered, the postulated flaw depth, and calculated K_I for all of the nozzles investigated.

Also given in Table 4 is the ratio between the K_I calculated using the corrected path stresses taken from the 2-D FEA and the path stresses taken from the 3-D FEA. The results in Table 4 indicate that when the 2-D corrected path stresses are in agreement with the 3-D path stresses, the calculated stress intensity factors also agree; however, when the stress correction is poor, the calculated stress intensity factors also do not agree, as would be expected since K_I is proportional to stress. Consequently, it is expected that the 2-D stress results for the CE RPV Outlet and W RPV SI nozzles will not result in K_I values that agree with those calculated using the 3-D FEA stress results, as shown in Table 4. Further, the B&W RPV Core Flood and B&W RPV Inlet nozzles are expected to show good agreement between the K_I values calculated using the corrected 2-D or the 3-D stresses. This is also shown in Table 4.

TABLE 4: SUMMARY OF NOZZLE FRACTURE MECHANICS RESULTS

	C0	C1	C2	C3	a, in (Note 2)	K_{IP}, ksi-in$^{0.5}$ (Note 3)	Ratio ($K_{I,2D}/K_{I,3D}$)
CE Outlet (Note 1)	28.744	-1.1189	0.0575	0.013	4.78	73.6	1.29
	24.266	-1.9105	0.0942	-0.0024	5.02	56.9	
W SI (Note 1)	-5.0954	3.0168	0.6291	0.0549	1.02	-4.3	7.44
	-0.7465	0.5977	-0.0118	-0.0102	1.07	-0.6	
B&W Core Flood	20736	-3938.7	759.28	-63.519	4.45	41.4	1.06
	21317	-4994.4	929.2	-73.634	4.42	39.2	
B&W Inlet	20975	-1254	128.89	-6.5038	4.54	50.4	0.98
	22274	-2414.3	220.5	-11.265	5.54	51.5	

1. Path stresses are plotted in ksi; therefore, polynomial curve fit coefficients result in stresses with units of ksi.
2. ¼ wall thickness flaw depth defined as ¼ of the 45 degree path length.
3. $K_I = \sqrt{\pi a}\left[0.706A_0 + 0.537\left(\frac{2a}{\pi}\right)A_1 + 0.448\left(\frac{a^2}{2}\right)A_2 + 0.393\left(\frac{4a^3}{3\pi}\right)A_3\right]$

CE RPV OUTLET NOZZLE MODEL WITH A 3-D SIMULATED CIRCULAR CORNER CRACK

A 3-D FEM for the CE RPV Outlet nozzle including a circular nozzle corner crack was constructed using ABAQUS/CAE. The mesh included the same portions of the nozzle assembly as the uncracked 3-D FEM. The postulated 1/4t circular corner crack included in the FEM is shown in Figure 20.

The 3-D FEM for the CE RPV Outlet nozzle with a postulated 1/4t circular corner crack was subjected to 1,000 psig internal pressure loading. Figure 21 displays the K_I values along the crack front from the nozzle inner surface side of the crack to the RPV wall side of the crack. Similar results as those obtained for the other nozzles [8] were observed for the CE RPV Outlet nozzle: the lowest value of K_I occurs near the middle of the circular crack front; the magnification factor method solution result (the square point in Figure 21) using Equation (4) is bounding compared with the 3-D finite element solution at the deepest point of the crack; the magnification factor method solution does not bound the maximum K_I at the ends of the crack; and, the deepest point magnification factor method solution for 1/4t flaw bounds the entire estimated crack front solution for a more reasonably-sized 0.1t flaw. Therefore, similar to the conclusions made for the nozzles in Reference [8], the conservatism of assuming a 1/4t flaw bounds the potential non-conservatism of evaluating only the deepest point of the crack, and, as part of using the simplified magnification factor method solution, it is important to maintain the use of a large postulated flaw size. Any use of reduced flaw sizes should account for the variation in K_I along the face of the crack, as well as other potential sources of loading.

DISCUSSION

As shown in Table 3, the bounding CF suggested by Yin, et al. [8] and the method proposed by Sommerville and Walter [5] give a reasonable approximation of the CF for the total stress at the nozzle corner for all nozzles considered.

The approach of uniformly scaling the entire stress distribution by the CF is conservative, but not excessively so, over the first ¼ of the wall thickness for the Core Flood and Inlet nozzles considered, as shown in Figures 18 and 19. Further, the K_I calculated using the '2-D Corrected' stress distribution and the BIE/IF solution is within 6% of that calculated using the '3-D' stress distribution for both nozzles, as shown in Table 4.

In contrast, this approach is excessively conservative for the CE RPV Outlet Nozzle, as shown in Figure 16. This can be observed by reviewing the '2-D Corrected' and '3-D' path stresses in Figure 16. Further the '2-D corrected' stress gives a predicted K_I using the BIE/IF approach, which is 30% larger than that calculated using the '3-D' path stress, as shown in Table 4. It is also notable that the application of the uniform scaling factor approach does nothing to correct for the fact that the through wall stress distributions are substantially different in the '2-D' and '3-D' cases.

Review of the path stress distributions reported for the SI nozzle, shown in Figure 17, shows that application of a uniform CF completely misrepresents the through wall stress distribution. Rather than more closely approximating the 3-D path stress distribution, the CF approach effectively rotates the distribution (since it passes through zero and the positive stresses get more positive and the negative stresses get more negative). The resulting corrected stress distribution is neither appropriate nor acceptable for this nozzle design.

CONCLUSIONS

The results from this investigation of additional PWR nozzles are as follows:

1. For nozzles with geometries consistent with those for which the method in Reference [5] was developed (B&W RPV Core Flood and B&W RPV Inlet nozzles), the CF method gives an acceptable correction factor approach for use with 2-D axi-symmetric FEA stresses.
2. For nozzles with unique corner geometries that are inconsistent with those for which the CF method in Reference [5] was developed (CE RPV Outlet and W RPV SI nozzles), the CF method yields non-conservative CFs for use with 2-D stresses. It is overly conservative for the CE RPV Outlet nozzle and entirely incorrect for the SI nozzle.
3. The bounding correction factors of 3.1 for rounded inside corners and 3.5 for special discontinuities or sharp inside corners given in Yin, et al. [8] bound the CFs calculated for all of the nozzles evaluated in this investigation.
4. Neither the Outlet nor Safety Injection nozzles exhibit 2-D path stresses which are amenable to the simple correction approach used successfully for other LWR nozzle designs.
5. The unit pressure load stress distribution observed in the W RPV SI nozzle indicates that a nozzle corner crack location is not the appropriate location based on maximum stress that should be considered for analysis to assess RPV integrity, such as those performed to satisfy the intent of ASME Code, Section XI, Nonmandatory Appendix G. The highest stressed region for this nozzle design is in the nozzle bore. Thus, postulated cracking at the nozzle bore location is indicated; however, for the case where irradiation effects need to be considered, this location is not limiting from a materials viewpoint since it is further removed from the RPV core. Therefore, the selection of a limiting path is not obvious and should be decided on a nozzle-specific basis.
6. Additional FEA LEFM evaluations of nozzle corner crack configurations exhibit similar observations as those performed in Reference [8]; the BIE/IF nozzle corner crack solution gives a reasonable estimate of the K_I for postulated cracks on a 45 degree path at the nozzle corner. The BIE/IF solution was developed such that it essentially estimates an average K_I along the entire crack front; thus, comparisons between the BIE/IF K_I and average FEA LEFM K_I are expected to show good agreement, as suggested by the comparison given in Figure 21.

It is recognized that no evaluation has been done as a part of this investigation regarding anticipated thermal loading or neutron embrittlement. Both of these must be considered appropriately when performing ASME Code, Section XI, Nonmandatory Appendix G analyses.

DISCLAIMER

This paper provides interim research results from an ongoing research project being conducted under NRC contract at the Oak Ridge National Laboratory. The views expressed herein are those of the authors and should not be construed as the United States Nuclear Regulatory Commission's official position. This manuscript has been authored by UT-Battelle, LLC, under contract DE-AC05-00OR22725 with the U. S. Department of Energy. The United States Government retains and the publisher, by accepting the article for publication, acknowledges that the United States Government retains a non-exclusive, paid-up, irrevocable, world-wide license to publish or reproduce the published form of this manuscript, or allow others to do so, for United States Government purposes.

REFERENCES

1. Wichman, K. R., Hopper, A. G., Mershon, J. L., "Local Stresses in Spherical and Cylindrical Shells due to External Loadings," Welding Research Council Bulletin 107, August 1965.
2. Mokhtarian, K., Endicott, J. S., "Stresses in Intersecting Cylinders Subjected to Pressure," Welding Research Council Bulletin 368, November, 1991.
3. Walter, M. C., Sommerville, D. V., *Nozzle Blend Radius Peak Stress Correction Factors for 2-D Axisymmetric Finite Element Models*, PVP2010—25104, Proceedings of the 2010 PVP Conference.
4. *BWRVIP-108: BWR Vessel and Internals Project, Technical Basis for the Reduction of Inspection Requirements for the Boiling Water Reactor Nozzle-to-Vessel Shell Welds and Nozzle Blend Radii*, EPRI, Palo Alto, CA 2002. 1003557.
5. Sommerville, D., Walter, M., *An Investigation into the Effects of Modeling Cylindrical Nozzle to Cylindrical*

Vessel Interactions Using 2D Axisymmetric Finite Element Models and a Proposed Method for Correcting the Results, PVP2011-57001, Proceedings of the 2011 PVP Conference.

6. Truitt, J. B., Raju, P. P., *Three-Dimensional versus Axisymmetric Finite-Element Analysis of a Cylindrical Vessel Inlet Nozzle Subject to Internal Pressure – A Comparative Study*, Transactions of the ASME, May 1978, Vol. 100, pp 134-140.
7. Mehta, H. S., Griesbach, T. J., Stevens, G. L., *Suggested Improvements to Appendix G of ASME Section XI Code*, PVP2008-61624, Proceedings of the 2008 PVP Conference.
8. Yin, S., Stevens G. L., Bass, B. R., and Kirk, M. T., *Stress and Fracture Mechanics Analyses of Boiling Water Reactor and Pressurized Water Reactor Vessel Nozzles*, PVP2011-57014, Proceedings of the 2011 PVP Conference.
9. Pilkey, W. D., Pilkey, D. F., Peterson's Stress Concentration Factors, 3rd. Ed., John Wiley & Sons, 2008.
10. Van Dyke, P., 1965, *Stresses about a circular hole in a cylindrical shell*, AIAA J., Vol. 3, p. 1733.
11. American Society of Mechanical Engineers Boiler and Pressure Vessel Code, 2011 Addenda, Section III, Rules for Construction of Nuclear Facility Components, New York.
12. ABAQUS Finite Element Software, Version 6.9, Dassault Simulia Corp., 2009.
13. ANSYS Mechanical APDL and PrepPost, Release 12.1 x64, ANSYS, Inc., November 2009.
14. Mehta, H. S., Griesbach, T. J., Stevens, G. L., *Suggested Improvements to Appendix G of ASME Section XI Code*, PVP2008-61624, Proceedings of the 2008 PVP Conference.
15. Mehta, H., et. al., *Additional Improvements to Appendix G of ASME Section XI Code for Nozzles*, PVP2011-57015, Proceedings of the 2011 PVP Conference.
16. Delvin, S. A. and Riccardella, P. C., June 25-30, 1978, "Fracture Mechanics Analysis of JAERI Model Pressure Vessel Test," Proceedings of the 1978 ASME Pressure Vessels and Piping Conference, Montreal, Quebec, Canada, Paper No. 78-PVP-91.

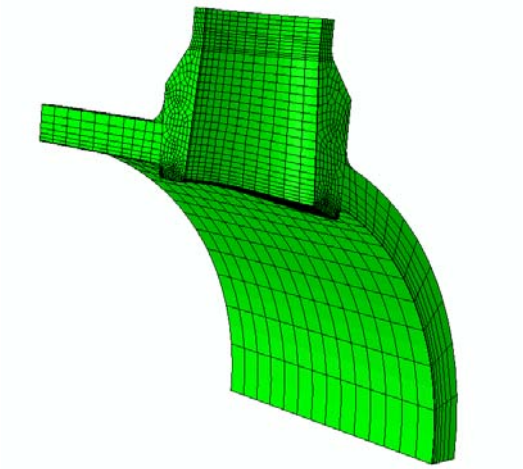

FIGURE 5: CE OUTLET NOZZLE 3-D FEM

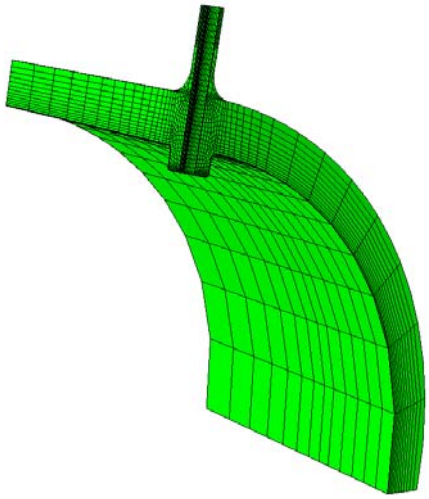

FIGURE 6: WESTINGHOUSE SI NOZZLE 3-D FEM

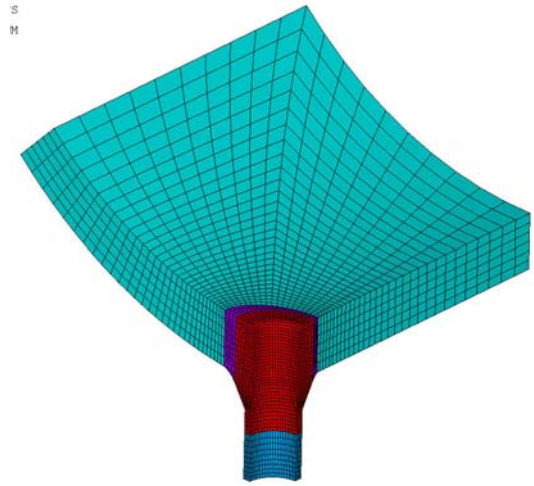

FIGURE 7: B&W CORE FLOOD NOZZLE 3-D FEM

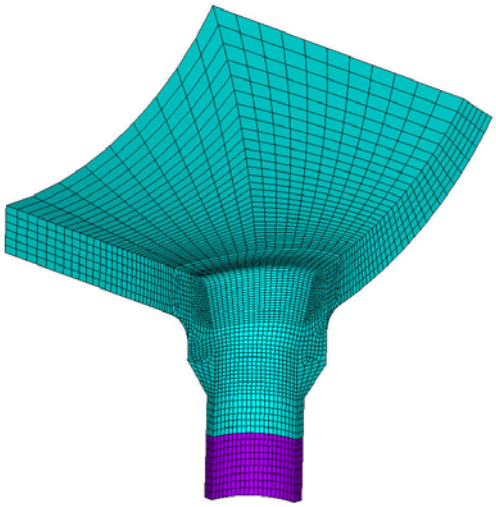

FIGURE 8: B&W INLET NOZZLE 3-D FEM

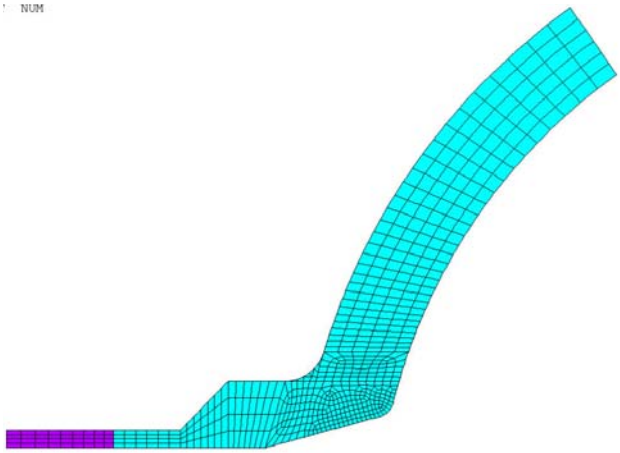

FIGURE 9: B&W INLET NOZZLE 2-D FEM

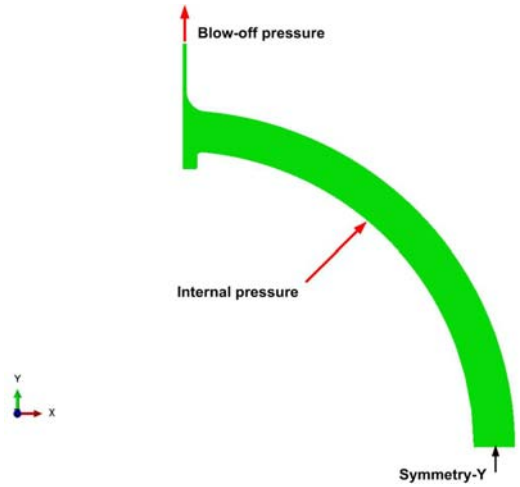

FIGURE 10: BOUNDARY CONDITIONS AND LOADS FOR 2-D MODELS

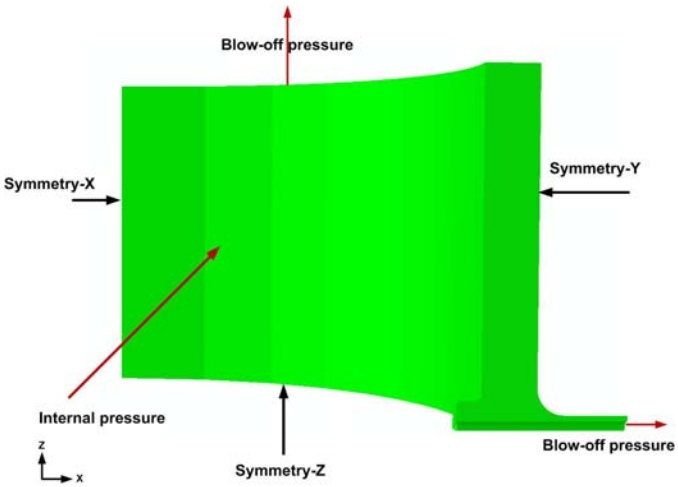

FIGURE 11: BOUNDARY CONDITIONS AND LOADS FOR 3-D MODELS

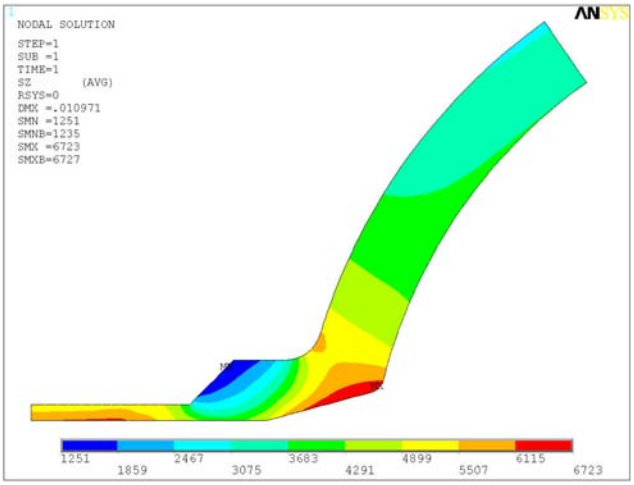

FIGURE 12: B&W INLET NOZZLE 2-D HOOP STRESS

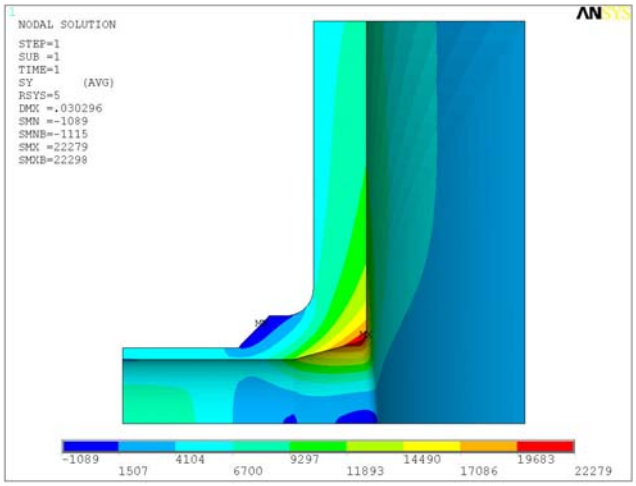

FIGURE 13: B&W INLET NOZZLE 3-D HOOP STRESS

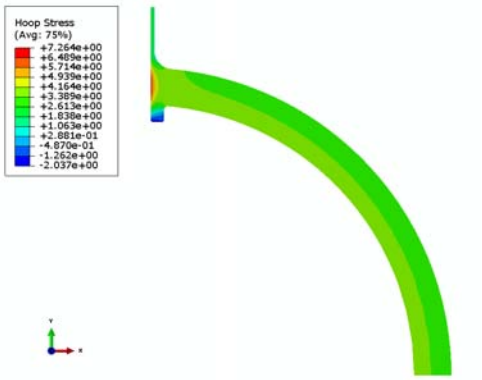

FIGURE 14: WESTINGHOUSE SI NOZZLE 2-D HOOP STRESS

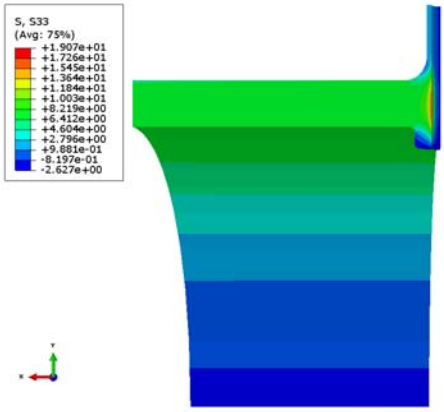

FIGURE 15: WESTINGHOUSE SI NOZZLE 3-D HOOP STRESS

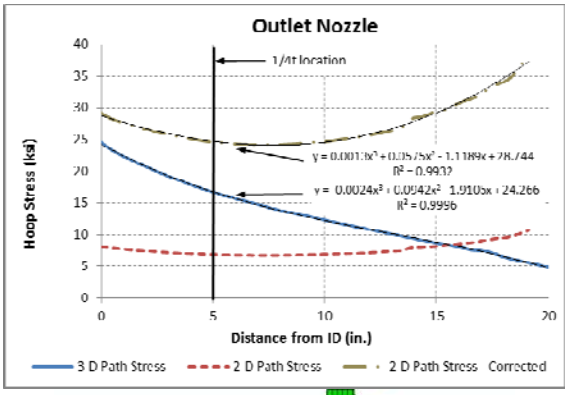

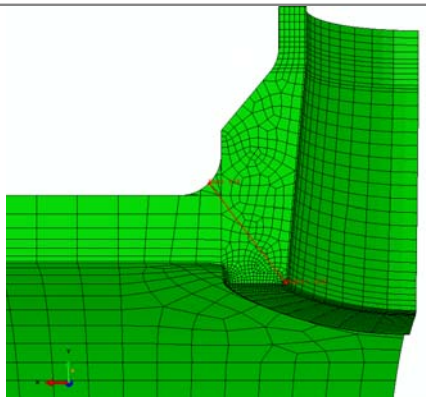

FIGURE 16: CE OUTLET NOZZLE PATH STRESSES

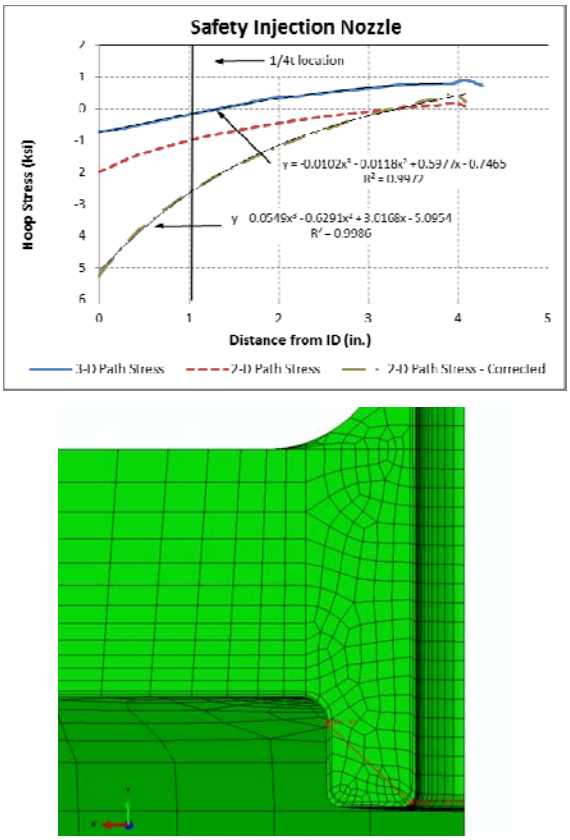

FIGURE 17: WESTINGHOUSE SI NOZZLE PATH STRESSES

FIGURE 18: B&W CORE FLOOD NOZZLE PATH STRESSES

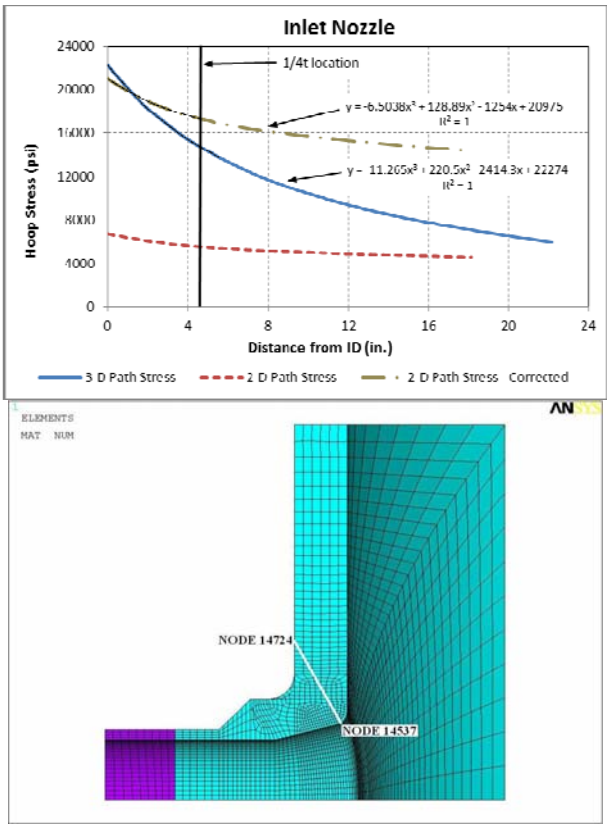

FIGURE 19: B&W INLET NOZZLE PATH STRESSES

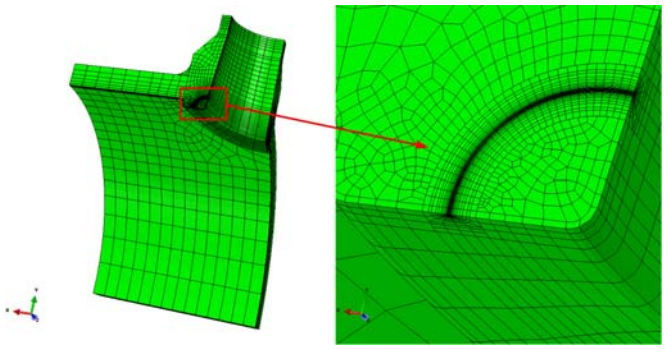

FIGURE 20: CE OUTLET NOZZLE CRACK MESH

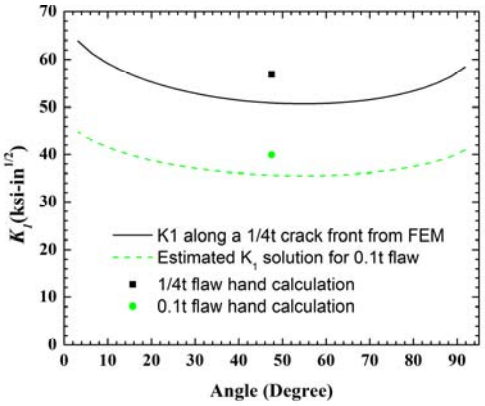

FIGURE 21: KI DISTRIBUTION FOR CE OUTLET NOZZLE, ¼ CIRCULAR CRACK FRONT, ¼T FLAW DEPTH